Research Article

Mirza Nadeem Ahmad, Arif Hussain, Muhammad Naveed Anjum*, Tajamal Hussain, Adnan Mujahid, Muhammad Hammad Khan*, Toheed Ahmed

Synthesis and characterization of a novel chitosan-grafted-polyorthoethylaniline biocomposite and utilization for dye removal from water

https://doi.org/10.1515/chem-2020-0137
received November 28, 2019; accepted May 12, 2020

Abstract: Chitosan was grafted with polyorthoethylaniline through oxidative polymerization using ammonium persulfate as oxidant, resulting in the formation of a biocomposite of chitosan-grafted-polyorthoethylaniline (CH-*g*-POEA). The synthesized biocomposite (CH-*g*-POEA) was characterized by FTIR, SEM, and TGA. Adsorption of methyl orange (MO) dye by CH-*g*-POEA was studied, wherein the Langmuir isotherm model with a R^2 of 0.9979 and adsorption capacity of 45.7 mg/g was evaluated.

Keywords: biopolymer, biocomposite, adsorption, chitosan, polyorthoethylaniline

1 Introduction

Biocomposites of synthetic and natural polymers have gained much attention during the last decade due to their versatile properties such as biocompatibility, biodegradability, and eco-friendly nature [1–3]. Biocomposites have been employed to remove toxic contaminants from polluted water [4–6]. Chitosan has unique characteristics of being antifungal [7,8], antimicrobial [9], and biodegradable properties [10]. Therefore, chitosan is a preferred biomaterial for the fabrication of composites with multipurpose applications in different aspects of life ranging from biomedicine to electronics [11]. Chitosan grafted with various synthetic polymers showed good adsorption ability for different organic dyes and is used to remove them from polluted water [12,13]. Composites of conducting polymers grafted onto chitosan have been reported to show a good pH sensing characteristic and are used as sensors [14]. Khan and Dhayal prepared a hybrid conducting film of chitosan-based material on an indium tin oxide electrode with the help of electrochemical polymerization that has potential application as biosensor to detect ochratoxin-A [15]. A hybrid complex of chitosan and polyaniline synthesized by the insertion of $ZnCl_2$ increased the adsorption capability toward reactive dyes [16]. Chitosan–polyaniline matrix and complexes have also been reported to act as absorbent for the separation of dye, lead and cadmium ions from water to reduce water pollution [17,18].

In this work, a chitosan-based biocomposite has been fabricated by grafting polyorthoethylaniline (CH-*g*-POEA) on a chitosan backbone and is used as an adsorbent for the dye. Adsorption kinetics and isotherms have been studied. It was found that the biocomposite of chitosan (CH-*g*-POEA) possesses the potential to adsorb and remove the dye from polluted water showing to be a good adsorbent.

2 Experimental section

2.1 Materials and methods

Chitosan (85% deacetylated) was purchased from Shanghai Aladdin Bio-Chem Technology Co., Ltd, China. Monomer, *o*-ethylaniline, methyl orange (MO), and oxidant, ammonium persulfate, were purchased from Sigma-Aldrich Co. An initiator, diaminodiphenylamine (DDPA), was supplied by Tokyo Chemical Industry, Shanghai. Preparation of reagents and washing of products were done in double distilled water.

* **Corresponding author: Muhammad Naveed Anjum,** Department of Applied Chemistry, Government College University Faisalabad, Faisalabad 38000, Pakistan, e-mail: anjumccj@hotmail.com
* **Corresponding author: Muhammad Hammad Khan,** Center for Environmental Protection Studied, PCSIR, Ferozepur Road, Lahore, Pakistan, e-mail: hammadchmst@gmail.com
Mirza Nadeem Ahmad, Arif Hussain, Toheed Ahmed: Department of Applied Chemistry, Government College University Faisalabad, Faisalabad 38000, Pakistan
Tajamal Hussain, Adnan Mujahid: Institute of Chemistry, University of the Punjab, Lahore 54000, Pakistan

2.2 Polymerization of *o*-ethylaniline

In the present experimental procedure, an amount of 0.24 mmol of *o*-ethylaniline was dissolved in 0.1 M HCl along with 0.01 mmol of DDPA and this solution was referred to as A. The second solution, referred to as B, was made by dissolving 0.24 mmol of APS in 0.1 M HCl. This solution B was poured and mixed in solution A by vigorous stirring. Afterwards, the polymerization process continued for 2 h. The resulting crude polymeric product obtained was washed using water and then separation was done by centrifugation [19].

2.3 Preparation of chitosan-*g*-polyorthoethylaniline

Chitosan-*g*-polyorthoethylaniline (CH-*g*-POEA) biocomposite was synthesized by oxidative polymerization of chitosan and *o*-ethylaniline monomer, in which an acidic solution of 0.1 M HCl and 20% acetic acid was used to dissolve *o*-ethylaniline and chitosan [20]. Solution A contained varying amounts of chitosan (0.1, 0.5, and 1 g) in a 20% acetic acid solution and was stirred for 4 h constantly. Solution B was prepared by adding 12 mL of 0.01 M *o*-ethylaniline and 7 mL of 0.0001 M DDPA in 0.1 M HCl. Then, solution C was prepared by adding 4 g of APS in 0.1 M HCl (7 mL). After this, solutions A and B were mixed with constant stirring of 15 min at 25°C. Finally, solution C was added dropwise and the resulting reaction mixture was stirred for 2 h. A greenish color solution was obtained, indicating the polymerization. After polymerization, each composite polymer was washed by centrifugation at 5,000 rpm for 5 min with water and then with methanol to remove byproducts before finally drying in an oven at 60°C for 90 min. CH-*g*-POEA samples were characterized by different characterization methods such as UV-visible, FTIR, TGA, and SEM analysis (Scheme 1).

2.4 Adsorption experiments

As a model pollutant dye, MO was used for the adsorption experiment and MO stock solution, 500 mg L^{-1} of MO, was made in double distilled water, which was then diluted to prepare the working solution (2.5–30 mg/L). For absorption maximum, the MO solutions were scanned by UV-vis spectrophotometric analysis in the range of 300–900 nm and the maximum absorbance (λ_{max}) was found at 464 nm. The absorbance (λ_{max}) of the dye (MO) was observed at 464 nm. To study adsorption kinetics, 30 mg/L of MO solution was added to 40 mg of

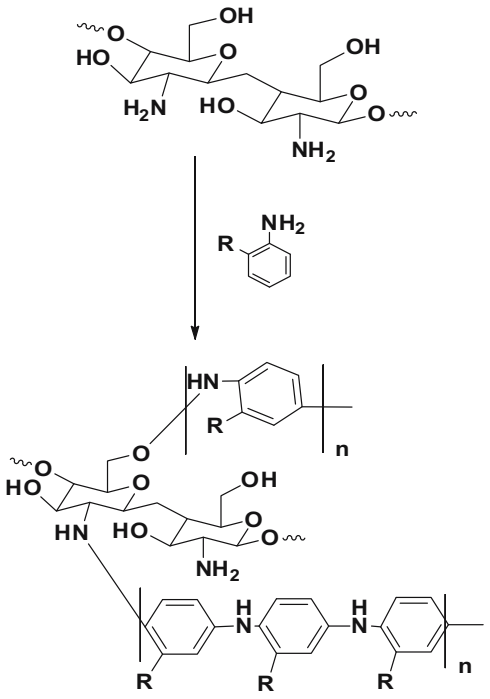

Scheme 1: Proposed scheme for the synthesis of chitosan-based CH-*g*-POEA.

CH-POEA and stirred. Predefined amount (2 mL) of the mixture was taken after specific time period of 4 min and centrifuged for 5 min at 5,000 rpm and then the absorbance was analyzed at 464 nm. The amount of dye, MO, in the supernatant solution was evaluated by UV-visible spectroscopy. During the isotherm adsorption experimental method, the contact time was fixed as 3 h and the

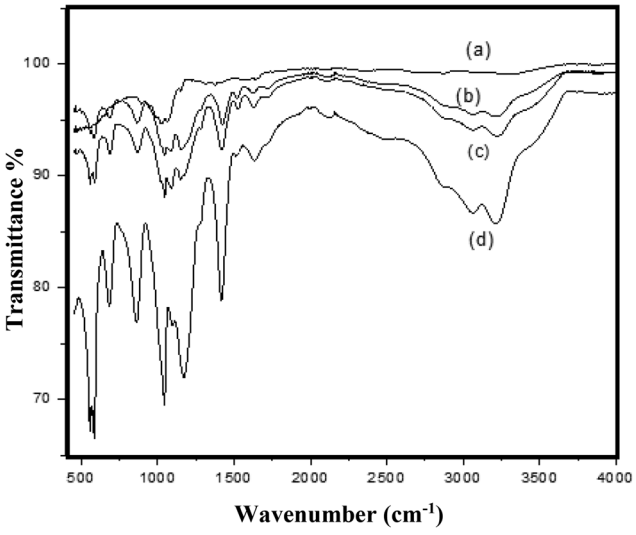

Figure 1: FTIR spectra of chitosan (a), 1 g CH-*g*-POEA (b), 0.5 g CH-*g*-POEA (c), and pure polyorthoethylaniline (d).

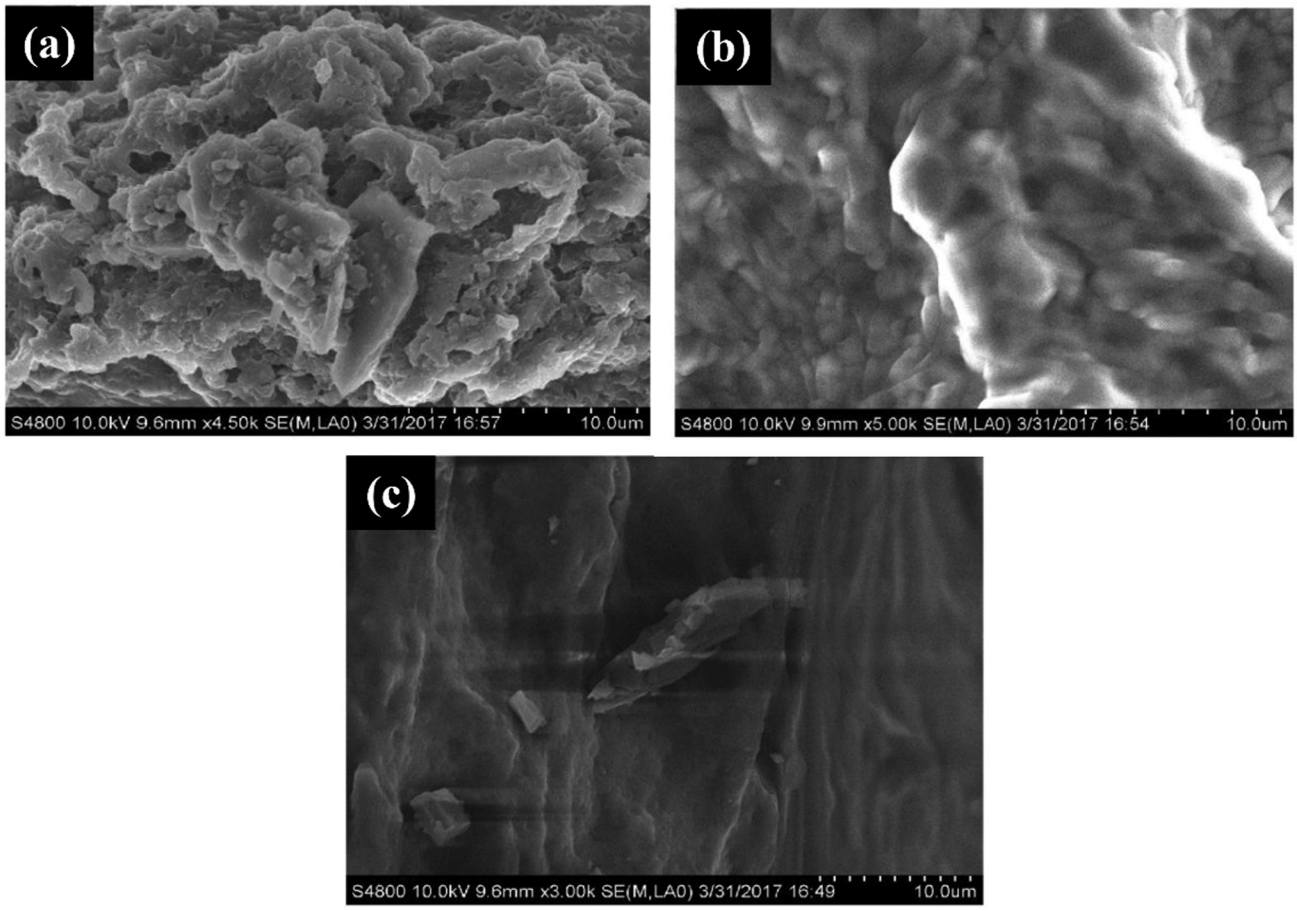

Figure 2: SEM of (a) pure POEA, (b) 0.5 g chitosan/CH-POEA composite, and (c) 1 g chitosan/CH-POEA.

amount of dye adsorbed onto CH-*g*-POEA biocomposite was calculated by using equation (1):

$$q_e = \frac{(C_0 - C_e)V}{m} \quad (1)$$

where q_e shows the amount of MO adsorbed onto per gram of CH-*g*-POEA biocomposite at equilibrium (mg g^{-1}), C_0 and C_e show the initial and equilibrium concentrations of MO (mg L^{-1}), respectively, and V indicates the volume of solution (L), while m is the mass of CH-*g*-POEA added [21].

Ethical approval: The conducted research is not related to either human or animal use.

3 Results and discussion

3.1 FTIR analysis

FTIR spectra of CH-*g*-POEA composites were recorded and the functional group peaks positions have been shown in Figure 1. The peaks of different compositions of chitosan and polyorthoethylaniline, such as 0.1, 0.5, and 1 g of chitosan, were observed. In Figure 1, the peaks at 830 cm^{-1}, 1,076^{-1}, and 3,371 represent the C–H bending, C–O stretching, and N–H stretching, respectively. A peak at 1,114 cm^{-1} in the CH-*g*-POEA composite, showing N═Q═N bonding, confirmed the reaction. No peak was detected in the CH-POEA spectrum at 1,114 cm^{-1}. In addition, 1,497 and 1,595 cm^{-1} showed stretching vibrations of the benzenoid ring and the quinoid ring, respectively. Moreover, peaks at 909 and 2,961 cm^{-1} are ascribed to C–H out-of-plane bending modes and C–H stretching of the ethyl group [4,22–24].

3.2 SEM morphology

The SEM images of pure ethylaniline and CH-*g*-POEA polymer composite are shown (Figure 2). The SEM image of a 9.8 mm composite was captured at different magnifications (×5,000, ×4,000, ×3,000). Figure 2(a) shows a porous

Table 1: BET analysis of the CH-*g*-POEA

Sample	BET surface area ($m^2\ g^{-1}$)	Average pore diameter (A)
CH-*g*-POEA	46.9	35.1

structure and Figure 2(b) shows the micrograph of CH-POEA (0.5 g chitosan) that revealed the interaction of chitosan and CH-POEA, and showed a compact structure. In Figure 2(c), the image of (1 g chitosan ratio) CH-POEA composite also showed POEA grafting on chitosan backbone. The BET surface area was determined from the nitrogen gas adsorption isotherm. According to the IUPAC standards, the BET results revealed the mesoporous structure of the sample. It also indicated that such porosity has better interaction with the dye molecules. Therefore, CH-*g*-POEA showed promising behavior toward efficient adsorption of the dye molecules. The calculated values are mentioned in Table 1.

3.3 TGA

Thermogravimetric study of the biocomposites of CH-*g*-POEA showed softening at 41°C and continued until 194°C. It lost 10.4% of its weight because of the removal of solvent and water contained between the polymeric chains. CH-*g*-POEA showed better stability below 200°C but above 210°C it started to degrade. Above 250°C, the polymeric chain starts to degrade and continued up to 400°C. The CH-*g*-POEA composite (1 g ratio) TGA showed an initial degradation temperature of (T_i) 247°C, polymer decomposition temperature of 267°C, and the maximum polymer decomposition temperature of (T_m) 329°C, respectively. The residual weight (γ_c) of the polymer at 599.04°C was found to be 45.07%. A comparison between changes in thermal resistance of CH-POEA and chitosan illustrates that the chitosan composite has more thermal resistance as a chitosan.

3.4 MO Adsorption on CH-*g*-POEA composite

Figure 4 illustrates the UV-visible spectra of increasing concentrations of MO solution ranging from 1.25–30 mg/L. The absorbance increases linearly by increasing the concentration of standard MO aqueous solution. A standard curve was plotted between the concentration

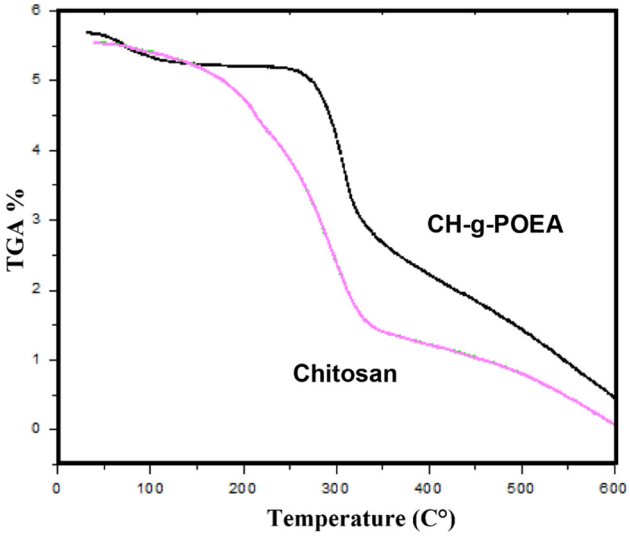

Figure 3: TGA of CH-*g*-POEA and chitosan.

and absorbance of MO that showed a straight line with a R^2 of 0.9965, a slope of 28.41, and an intercept at 0.68814 (Figure 4c).

In the kinetic study of the MO adsorption on CH-*g*-POEA composite, a graph of q_e/mg L^{-1} vs time that described the fast adsorption in the first several minutes was plotted. Then the q_e value increased slowly, until it became saturated. The graph indicated a very fast MO adsorption on polymer composite, which gradually decreased, until almost the equilibrium was reached at 40 m.

For the study of kinetics, adsorption experiments were carried out with different durations and fixed amount of biocomposite CH-*g*-POEA. Graphs were plotted for the pseudo-first-order and second-order kinetic studies. These parameters of $\log(q_e - at)$ and t/q_t were plotted vs time to apply the kinetic models of pseudo-first order and pseudo-second order. The R^2 values, revealed by the graph, are 0.9347 and 0.99945, which were obtained for pseudo-first-order and pseudo-second-order plots. The result obtained justifies that the second-order kinetics fitted well to the analyzed kinetic data of MO at room temperature for the biocomposite (CH-*g*-POEA). The result is validated by observing that the obtained value of q_e for the second-order kinetic model shows the closeness to the experiments. Results revealed that the adsorption process followed pseudo-second-order kinetics. Figure 4(c) shows that in the first 50 min, the adsorption process is fast and then continued to increase slowly. Figure 5(b) shows the pseudo-second-order kinetic plot for the adsorption of CH-*g*-POEA biocomposite according to the pseudo-second-order equation:

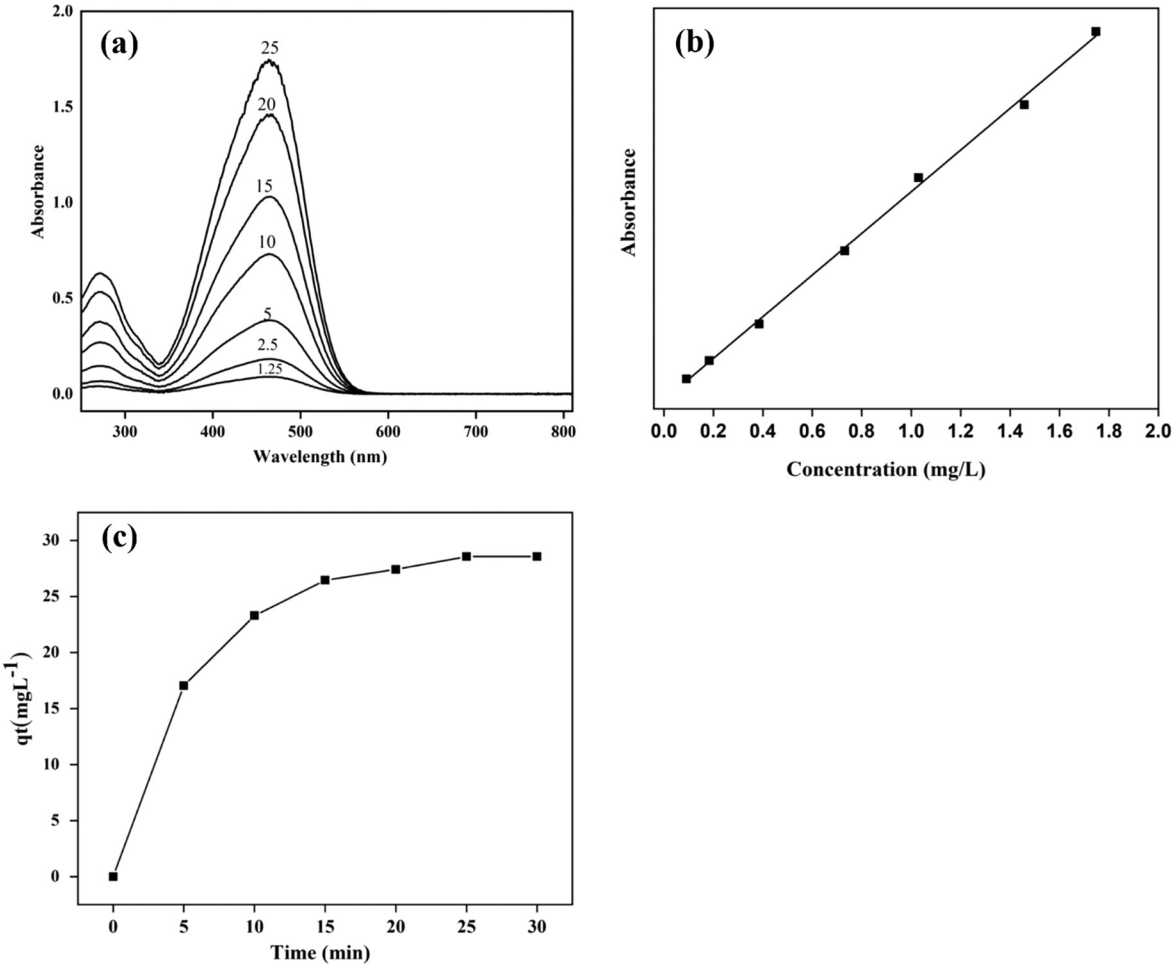

Figure 4: (a) UV-visible spectra of different concentrations (mg/L) of the MO solution, (b) linear fit, and (c) kinetics of MO adsorption on CH-*g*-POEA.

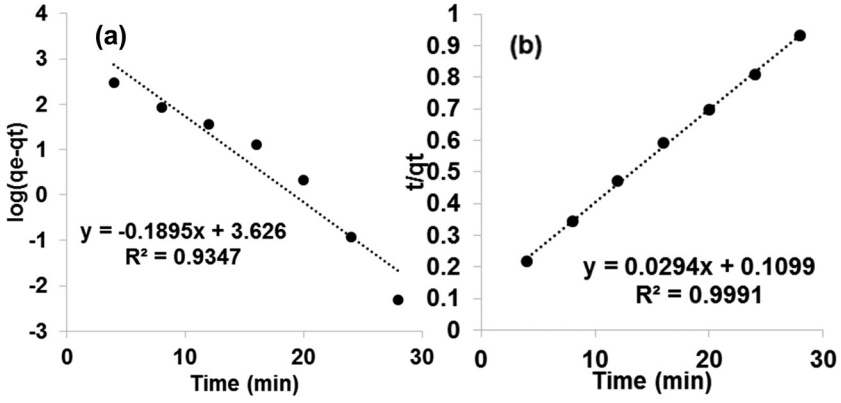

Figure 5: (a) Pseudo-first-order- and (b) pseudo-second-order kinetics for the uptake of MO by biocomposite.

$$\frac{t}{q_t} = \frac{1}{k_2 q_e^2} + \frac{t}{q_e} \quad (2)$$

where q_e and q_t show the amounts (mg g^{-1}) of MO adsorbed onto CH-*g*-POEA biocomposite at equilibrium and at time t (min), respectively, while k_2 is the rate constant (g mg^{-1} min). Similarly, the plot of t/q_e and t is linear having a value of $R^2 = 0.9991$. This reveals that the adsorption of the dye MO by CH-*g*-POEA biocomposite is explained by the pseudo-second-order model.

The adsorption data were used to find out the relationship between the adsorbed (q_e) and aqueous

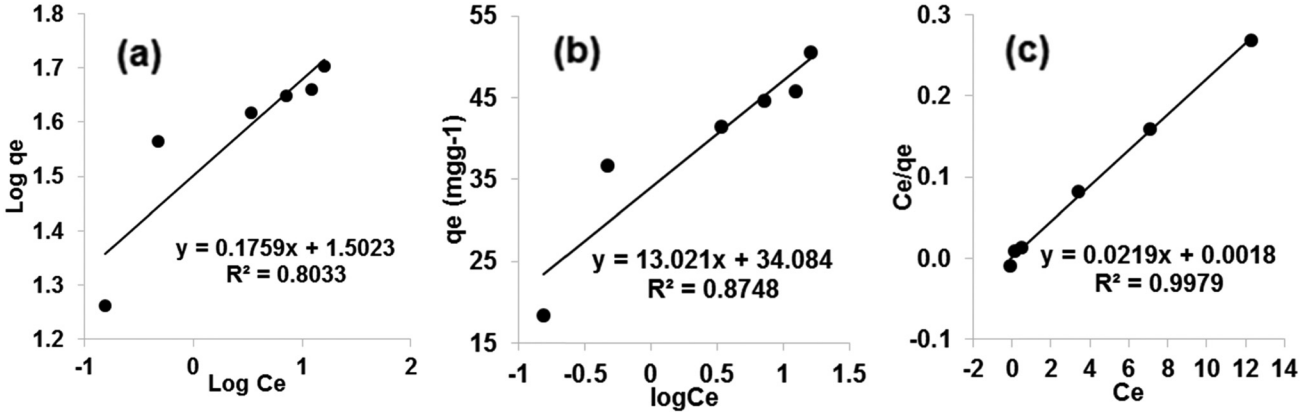

Figure 6: Isotherm models for MO adsorption on CH-*g*-POEA: (a) Freundlich, (b) Temkin, and (c) Langmuir.

concentration (C_e) of biocomposite by isotherm models, i.e., Langmuir, Freundlich, and Temkin models. The experimental equilibrium adsorption data were analyzed by using the Langmuir equation and Temkin equation (3):

$$\frac{C_e}{q_e} = \frac{1}{q_m k_L} + \frac{C_e}{q_m} \tag{3}$$

$$\log q_e = \log k_f + 1/n \log c_e \tag{4}$$

where q_m shows the maximum monomolecular adsorption capacity (mg g^{-1}) and k_L the Langmuir constant (L mg^{-1}).

The resultant correlation values R^2 for Freundlich and Temkin isotherm models were 0.8033 and 0.8748. It showed that the MO adsorption did not follow the Freundlich and Temkin isotherm assumptions. The correlation value of R^2 for the Langmuir model was 0.9979 with adsorption capacity of 45.7 mg/g. It proved that the adsorption of the MO dye followed the Langmuir modelassumptions.

The Freundlich isotherm is a model that was applicable for the low concentration range that does not show a finite uptake capacity of the sorbent. The Temkin isotherm explains the adsorbent–adsorbate interaction. It justifies the adsorption mechanism by the uniform surface due to the binding energies.

The Langmuir isotherm gives an explanation for the uptake capability of the adsorbent at the equilibrium position. The isotherm justifies that the adsorption mechanism is restricted to a single layer, because the available vacant sites were filled by the sorbed molecules and were not able to exert further force of attraction. The Langmuir isotherm clarifies that the uptake of dye molecule takes place homogenously throughout the monolayer adsorbent surface.

If the MO molecules are taken up independently on a single type of binding site in such a way that the uptake of the first dye molecule does not affect the sorption of the next molecule, then the sorption process would follow the Langmuir adsorption isotherm. Hence, the prepared biocomposite CH-*g*-POEA followed the pseudo-second-order kinetics for the MO adsorption, showing that the adsorption was dependent upon the chemical interaction between the adsorbate and the adsorbent. The adsorption on the MO followed the Langmuir model of adsorption isotherm and CH-*g*-POEA showed a better adsorption than many previously reported adsorbents such as modified sporopollenin, activated carbon, orange peel, banana peel, and POC microsphere [25–27].

4 Conclusion

Grafting of chitosan with polyorthoethylanline was carried out via oxidative polymerization using ammonium persulfate as oxidant and DDPA as initiator resulting in the formation of biocomposite (CH-*g*-POEA). Grafted chitosan (CH-*g*-POEA) was characterized by FTIR, SEM, and TGA. Moreover, adsorption of MO by CH-*g*-POEA was evaluated and it was revealed by the Langmuir isotherm model that the adsorption capacity was 45.7 mg/g. In short, CH-*g*-POEA biocomposite can be a cost-effective material for the separation and removal of dyes MO from polluted industrial effluents.

Acknowledgment: Authors are thankful to Hi-Tech Laboratory, GC University, Faisalabad, Pakistan.

Conflict of interest: Authors declare no conflict of interest.

References

[1] Igberase E, Osifo P. Equilibrium, kinetic, thermodynamic and desorption studies of cadmium and lead by polyaniline grafted cross-linked chitosan beads from aqueous solution. J Ind Eng Chem. 2015;26:340–7.

[2] Ismail YA, Shin SR, Shin KM, Yoon SG, Shon K, Kim SI, et al. Electrochemical actuation in chitosan/polyaniline microfibers for artificial muscles fabricated using an in situ polymerization. Sens Actuators B. 2008;129(2):834–40.

[3] Wang J, Deng B, Chen H, Wang X, Zheng J. Removal of aqueous Hg(II) by polyaniline: sorption characteristics and mechanisms. Environ Sci Technol. 2009;43(14):5223–8.

[4] Bhaumik M, Maity A, Srinivasu V, Onyango MS. Removal of hexavalent chromium from aqueous solution using polypyrrole-polyaniline nanofibers. Chem Eng J. 2012;181:323–33.

[5] Karthikeyan M, Kumar KS, Elango K. Batch sorption studies on the removal of fluoride ions from water using eco-friendly conducting polymer/bio-polymer composites. Desalination. 2011;267(1):49–56.

[6] Shukla SK, Mishra AK, Arotiba OA, Mamba BB. Chitosan-based nanomaterials: a state-of-the-art review. Int J Biol Macromol. 2013;59:46–58.

[7] Aranaz I, Mengíbar M, Harris R, Paños I, Miralles B, Acosta N, et al. Functional characterization of chitin and chitosan. Curr Chem Biol. 2009;3(2):203–30.

[8] Zhao X, Li P, Guo B, Ma PX. Antibacterial and conductive injectable hydrogels based on quaternized chitosan-graft-polyaniline/oxidized dextran for tissue engineering. Acta Biomater. 2015;26:236–48.

[9] Sudarshan N, Hoover D, Knorr D. Antibacterial action of chitosan. Food Biotechnol. 1992;6(3):257–72.

[10] Vårum KM, Myhr MM, Hjerde RJ, Smidsrød O. In vitro degradation rates of partially *N*-acetylated chitosans in human serum. Carbohydr Res. 1997;299(1–2):99–101.

[11] Karthik R, Meenakshi S. Facile synthesis of cross linked-chitosan-grafted-polyaniline composite and its Cr(VI) uptake studies. Int J Biol Macromol. 2014;67:210–9.

[12] Sadeghi S, Fooladi E, Malekaneh M. A new amperometric biosensor based on Fe_3O_4/polyaniline/laccase/chitosan biocomposite-modified carbon paste electrode for determination of catechol in tea leaves. Appl Biochem Biotechnol. 2015;175(3):1603–16.

[13] Wang X, Yang T, Feng Y, Jiao K, Li G. A novel hydrogen peroxide biosensor based on the synergistic effect of gold-platinum alloy nanoparticles/polyaniline nanotube/chitosan nanocomposite membrane. Electroanal Int J Devot Fundam Pract Asp Electroanal. 2009;21(7):819–25.

[14] Kumar R, Oves M, Almeelbi T, Al-Makishah NH, Barakat M. Hybrid chitosan/polyaniline-polypyrrole biomaterial for enhanced adsorption and antimicrobial activity. J Colloid Interface Sci. 2017;490:488–96.

[15] Khan R, Dhayal M. Chitosan/polyaniline hybrid conducting biopolymer base impedimetric immunosensor to detect Ochratoxin-A. Biosens Bioelectron. 2009;24(6):1700–5.

[16] Kannusamy P, Sivalingam T. Synthesis of porous chitosan–polyaniline/ZnO hybrid composite and application for removal of reactive orange 16 dye. Colloids Surf B. 2013;108:229–38.

[17] Janaki V, Oh B-T, Shanthi K, Lee K-J, Ramasamy A, Kamala-Kannan S. Polyaniline/chitosan composite: an eco-friendly polymer for enhanced removal of dyes from aqueous solution. Synth Met. 2012;162(11–12):974–80.

[18] Karthik R, Meenakshi S. Removal of Pb(II) and Cd(II) ions from aqueous solution using polyaniline grafted chitosan. Chem Eng J. 2015;263:168–77.

[19] Anjum MN, Zhu L, Luo Z, Yan J, Tang H. Tailoring of chiroptical properties of substituted polyanilines by controlling steric hindrance. Polymer. 2011;52(25):5795–802.

[20] Tiwari A, Singh V. Synthesis and characterization of electrical conducting chitosan-graft-polyaniline. Express Polym Lett. 2007;1(5):308–17.

[21] Anjum MN, Zia KM, Zhu L, Ahmad MN, Zuber M, Tang H. Adsorption of methyl orange using self-assembled porous microspheres of poly(*o*-chloroaniline). Korean J Chem Eng. 2014;31(12):2192–7.

[22] Gandhi MR, Meenakshi S. Preparation and characterization of La(III) encapsulated silica gel/chitosan composite and its metal uptake studies. J Hazard Mater. 2012;203:29–37.

[23] Guo X, Fei GT, Su H, De Zhang L. High-performance and reproducible polyaniline nanowire/tubes for removal of Cr(VI) in aqueous solution. J Phys Chem C. 2011;115(5):1608–13.

[24] Butoi B, Groza A, Dinca P, Balan A, Barna V. Morphological and structural analysis of polyaniline and poly(*o*-anisidine) layers generated in a DC glow discharge plasma by using an oblique angle electrode deposition configuration. Polymers. 2017;9(12):732.

[25] Annadurai G, Juang R-S, Lee D-J. Use of cellulose-based wastes for adsorption of dyes from aqueous solutions. J Hazard Mater. 2002;92(3):263–74.

[26] Ayar A, Gezici O, Küçükosmanoğlu M. Adsorptive removal of methylene blue and methyl orange from aqueous media by carboxylated diaminoethane sporopollenin: on the usability of an aminocarboxilic acid functionality-bearing solid-stationary phase in column techniques. J Hazard Mater. 2007;146(1–2):186–93.

[27] Singh KP, Mohan D, Sinha S, Tondon G, Gosh D. Color removal from wastewater using low-cost activated carbon derived from agricultural waste material. Ind Eng Chem Res. 2003;42(9):1965–76.